coatings

MDPI

*Article*

# Plasma-Sprayed Hydroxyapatite Coatings and Their Biological Properties

**Szymon Kowalski [1,*], Weronika Gonciarz [2,*], Radosław Belka [3], Anna Góral [4], Magdalena Chmiela [2], Łukasz Lechowicz [5], Wiesław Kaca [5] and Wojciech Żórawski [1]**

1 Faculty of Mechatronics and Mechanical Engineering, Kielce University of Technology, 25-314 Kielce, Poland
2 Department of Immunology and Infectious Biology, Faculty of Biology and Environmental Protection, University of Łódź, 90-237 Łódź, Poland
3 Faculty of Electrical Engineering, Automatic Control and Computer Science, Kielce University of Technology, 25-541 Kielce, Poland
4 Institute of Metallurgy and Materials Science, Polish Academy of Sciences, 30-059 Kraków, Poland
5 Department of Microbiology, Institute of Biology, Jan Kochanowski University, 25-406 Kielce, Poland
* Correspondence: skowalski@tu.kielce.pl (S.K.); weronika.gonciarz@biol.uni.lodz.pl (W.G.)

**Abstract:** Air plasma spraying (APS) is a common method of producing hydroxyapatite (HA) coatings for alloprosthetic implants. Modification of HA spraying potentially may diminish the risk of inflammation and local infection during bone implantation. Titanium implants were HA coated with different deposition process parameters. HA powder was deposited using APS with axial powder injection at three different distances (100, 120, and 140 mm). The surface morphology of each implant was examined and the direct contact cytotoxicity of each HA coating was evaluated according to norm ISO 10993 5:2009. The response of monocytes to HA was assessed via the activation of transcription nuclear factor. All coatings had a lamellar structure. HA sprayed at a distance of 120 mm showed the highest roughness and little phase change. The analysis of the results of the conducted research showed that plasma-spraying distance during the HA coating process had a negligible impact on biocompatibility. The results obtained for a distance of 120 mm showed a slight increase in the biological properties tested. Moreover, HA coatings sprayed at different distances were not cytotoxic and did not stimulate the NF-kB. Bare titanium was less susceptible to colonization by *Staphylococcus aureus* than HA-coated surfaces. HA constitutes a potentially good, low-cost, non-cytotoxic material for joint prostheses.

**Keywords:** hydroxyapatite; plasma spraying; biocompatibility



**Citation:** Kowalski, S.; Gonciarz, W.; Belka, R.; Góral, A.; Chmiela, M.; Lechowicz, Ł.; Kaca, W.; Żórawski, W. Plasma-Sprayed Hydroxyapatite Coatings and Their Biological Properties. *Coatings* **2022**, *12*, 1317. https://doi.org/10.3390/coatings12091317

Academic Editors: Qi Hua Fan and Simona Liliana Iconaru

Received: 5 July 2022
Accepted: 7 September 2022
Published: 9 September 2022



## 1. Introduction

Titanium (Ti) and its alloys are commonly used materials for alloprosthetic implants [1]. The implants can be fixed in the human body by mechanical methods (e.g., screws), chemical means (cements), or biological interactions (by adherence of cells to the implant surface). However, non-modified Ti and its alloys exhibit inherently poor osseointegration because formed passivation films on the surface have significantly different chemical compositions compared with the surrounding tissues. It inhibits the formation of fiber capsules around the biomedical implants [2,3]. Therefore, only mechanical osseointegration is presented between the pure Ti implants and surrounding tissues instead of a strong chemical bone-bonding. Moreover, the passivation layer may be peeled off and dissolved in the human body, leading to inflammation and other health problems.

To avoid adverse tissue reactions and improve the alloy-tissue compatibility, the deposition of additional bioinert materials as bioactive glasses or calcium phosphates is preferred [4,5]. Hydroxyapatite (HA) is the most attractive calcium phosphate used for osteointegration due to its beneficial calcium to phosphorus 5:3 ratio. This relationship accelerates the healing process after bone implantation [6–8]. HA occurs in the bones of

vertebrates (up to 85% by mass) and is mainly responsible for their mechanical strength. Human bones carry loads of very different amplitudes, occurring over a great number of cycles during their lifetime. An example of this phenomenon can be the one described by J. Jamari et al. [9]. Due to their mechanical and tribological properties, titanium alloys are in great demand in bone implantology [10]. For this reason, HA coatings deposited on titanium and its alloys have been extensively studied, and new methods for their fabrication have been proposed and developed. There are many methods of applying hydroxyapatite coatings on implants, such as chemical vapor deposition, physical vapor deposition, hot dip method, electrophoretic deposition, cold pressing and sintering, hydrothermal synthesis, or suspension plasma spraying [11–18].

Air plasma spraying (APS) is a common industrial method for the deposition of HA coatings due to its reliability, efficiency, and reasonable cost [4]. Moreover, plasma spraying is the only thermal-spray process that has been approved by the U.S. Food and Drug Administration (FDA) for use in the deposition of HA coatings for medical implants [19].

HA as a ceramic requires large amounts of heat to be melted down, the plasma flame is a good source. In plasma spraying techniques, the input material (which can be powder, precursor solution, or liquid suspension) is injected directly into plasma flame. The material entrained in the steam is heated and melted (partially or completely). The drops of coating material that hit the substrate stick to it and solidify to form a coating. Unlike air plasma spraying, which can be carried out in the atmosphere, some materials require a controlled atmosphere or vacuum chamber. Compared to other HA coating processes, APS is characterized by high speed, which makes it possible to obtain thick coatings and a very rough surface with a structure characteristic of thermally sprayed coatings. Moreover, recently, research has been started on plasma-sprayed coatings from suspensions containing very fine grains, which gives completely new properties [20,21].

Plasma spraying has limitations associated with the high solidification rate of feedstock and the formation of the amorphous phase, as well as the appearance of cracks or issues bonding between the HA layer and titanium [17,22]. Nevertheless, plasma-sprayed coatings are the subject of intense research over time. Okhi et al. examined interfacial strength of plasma-sprayed HA coatings and found that the blasting media had a significant impact [23]. Bovine-derived HA coatings were deposited by HVOF and plasma spraying by Clavio-Mejia et al. It turned out that such plasma-sprayed coatings had properties comparable to those sprayed with standard HA powders [24]. A significant improvement in the corrosion properties of plasma-sprayed coatings in simulated body fluid was achieved by Singh et al. by adding 2 wt% graphene nanoplatelets to HA feedstock [25]. Liu et al. used a new vapour-induced pore-forming atmospheric plasma spraying technique and obtained HA coatings with increased porosity and surface roughness [26].

APS deposition of HA coatings has been realized so far by the radial injection of powder, whereby the powder is fed perpendicular to or in the direction of the plasma stream [27–30]. Shamray et al. investigated plasma-sprayed HA coatings fabricated on pre-heated titanium alloy OT4-1 substrates. They observed the appearance of two new phases in the as-sprayed coating, namely tetracalcium phosphate (TTCP, $Ca_4(PO_4)_2O$) and calcium oxide (CaO) [28]. These were attributed to differentiated remelting of HA powder grains during spraying due to a temperature gradient across the plasma stream. Liu et al. reported differences in the microstructure of the coatings, depending on the spraying distance; specifically, with increasing plasma gun distance, the intensity of particle melting was seen to increase [30]. It was rationalized in terms of the longer time for which the HA grains remained in the plasma stream. In the APS process, the final result depends on many factors, including powder properties, spray parameters, and the applied plasma system. The degree of grain remelting has a significant impact on the microstructure, phase composition, and properties of the coating. When slightly overheated, it breaks down into simpler calcium phosphates, principally tricalcium phosphate (TCP, $Ca_3(PO_4)_2$), and TTCP. Higher temperatures can result in an amorphous calcium phosphate (ACP) phase in the coating [31]. The aspect of thermal degradation/deformation of HA powder was also

discussed in the authors' earlier work [32], where a set of hydroxyapatite (HA) coatings deposited on titanium substrate at different spray distances was investigated. The hydroxyl group concentration was investigated by studying the OH vibrational mode intensity in the Raman spectra. The Photoluminescence (PL) and UV-VIS Diffuse Reflectance Spectroscopy (DRS) studies showed an increase in the optical absorption coefficients in the UVA region, which are associated with a higher concentration of oxygen vacancies in phosphate groups. The observed dehydroxylation and deoxidation phenomena have been associated with the formation of alternative phosphates, in particular TCP and TTCP. The preferred spraying distance of 100–140 mm was recommended for future use due to the lowest intensity of the dehydroxylation phenomena.

Despite the rich literature on bioactive HA materials, obtaining homogeneous and topographically favorable coatings with proper Ca:P stoichiometry is still an open issue. On the other hand, problems associated with uneven melting of the powder in the plasma stream in the case of radial injection can be significantly reduced by using an axial injection system. It benefits from a more homogeneous heating effect of HA grains in the plasma stream, allowing the formation of a more homogeneous microstructure [20,33]. The second important factor is the roughness of the coating, which plays a key role in the tissue growth process [34]. The microstructure, porosity, phase composition, and roughness of the coating are the essential factors that determine its properties [4,20,35].

Plasma spraying has a number of associated limitations; the high solidification rate of feedstock and the formation of the amorphous phase, and the appearance of cracks or issues bonding between HA layer and titanium [21,22]. Nevertheless, plasma-sprayed HA coatings have been the subject of intense research over time [23–26]. Most of the research is related to the coatings in which the powder is introduced radially into the plasma stream. However, this process has inherent limitations in powder injection efficiency, and the quality of the powder used is also very important. Therefore, a much better solution is to use axial powder injection, which allows the powder to be introduced directly into the core of the plasma jet, where the temperature and velocity are the highest. Such a solution provides more uniform heating of the powder grains and minimizes the particle segregation, which is a common problem in radially fed plasma guns. The other advances include the high powder feed rate and high deposition efficiency, which is also important from an economic point of view. In the literature, there are no data on such HA coatings, therefore, the presented research is new.

However, traditional material characterization seems to be incomplete in assessing the final functionality of the coatings. They can also be extended to cytotoxicity and bioactivity studies, e.g., by observing the microorganisms' activity.

This paper reports the bioactive properties of plasma-sprayed HA coatings deposited by axial injection on titanium alloys at three different distances. The effects of plasma-spray distance on in vitro biocompatibility, cytotoxicity, and adhesion of *Staphylococcus aureus* bacterial cells to three HA coatings have been investigated.

## 2. Materials and Methods

The study was conducted according to the following scheme, presented below in Figure 1, which is described in more detail in this chapter.

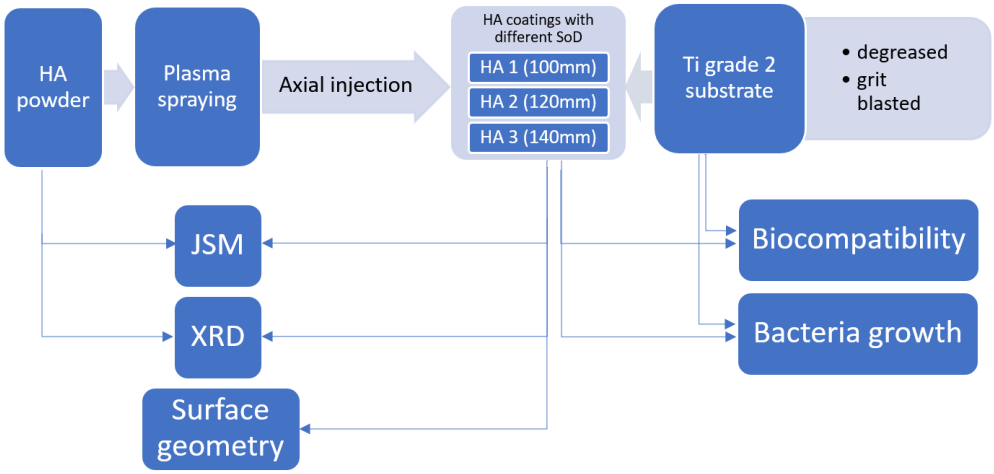


**Figure 1.** Workflow of the experiment.

### *2.1. HA Deposition and Characterization of HA Coatings*

HA coatings were deposited from XPT-D-703 powder (Sulzer Metco, Salzgitter, Germany) by a plasma-spraying process on 300 mm × 10 mm × 3 mm bars of grade 2 titanium on the one 300 mm × 10 mm side. The plasma-spraying process was performed by axial powder injection on an Axial III system (Northwest Mettech Corp., Surrey, Canada) with a Thermal Miller 1264 powder feeder. After deposition, bars were divided into smaller square samples with dimensions 10 mm × 10 mm with a diamond saw.

To assess the effect of the plasma-spray distance on the microstructural properties of the coating and its behavior in a specific biological environment, the process was carried out at distances of 100, 120, and 140 mm, and the obtained coatings were designated as HA1, HA2, and HA3, respectively. Before spraying, the substrates were degreased and sandblasted with EB-30 electrocorundum at a pressure of 0.5 MPa. The roughness of the surfaces after sandblasting was Sa = 4.919 µm. Parameters for the plasma spraying of HA powder are shown in Table 1. The thickness of the sprayed coatings was 0.2 mm.

**Table 1.** Plasma spraying parameters.

| Parameter | Value |
|---|---|
| Plasma gas flow (L/min) | 150 |
| Plasma gas composition (%) | 85 Ar/15 $H_2$ |
| Current (A) | 240 |
| Traverse gun speed (mm/s) | 200 |
| Spraying distances (mm) | 100, 120, 140 |

A JSM-7100 scanning microscope (JEOL, Inc., Peabody, MA, USA) was used to study the surface structures and morphologies of the surface of coatings and the adhesion of bacterial cells. Phase composition analysis of the HA powder and the sprayed coatings was performed using a Bruker D-8 Advance diffractometer (Bruker, Billerica, MA, USA). The surface topography of the sprayed coatings was examined using a Talysurf CCI-Lite 3D profilometer (Taylor Hobson, Warrenville, IL, USA).

### *2.2. Cell Culture and In Vitro Biocompatibility Assessment*

Reference L929 mouse fibroblasts (LGC Standards, Middlesex, UK) and human Hs68 skin fibroblasts (CRL-1635™) from American Type Cell Cultures (ATCC, Rockville, MD, USA), were cultured at 37 °C in a 5% $CO_2$ in Roswell Park Memorial Institute (RPMI)-1640 medium supplemented with 10% heat-inactivated fetal bovine serum (FBS), and standard antibiotics: penicillin (100 U/mL) and streptomycin (100 µg/mL), while the Hs68 cell line was grown in high glucose RPMI-1640 medium (Biowest, Nuaillé, France), containing 10%

FBS, 100 U/mL penicillin, and 100 µg/mL streptomycin (all cell culture components were from Biowest, Nuaillé, France). Cell cultures were supplemented with fresh medium two or three times per week to keep them in log phase. The confluent monolayer was treated with 0.25% trypsin-EDTA solution (Biowest, Nuaillé, France) to passage.

Biocompatibility of the HA coatings was tested using L929 and Hs68 cell line (density of $2 \times 10^5$ cells/mL) according to the ISO norm 10993-5 (International Organization for Standardization, 2009; Biological evaluation of medical devices—Part 5: Tests for in vitro cytotoxicity), based on the 3-(4,5-dimethylthiazol-2-yl)-2,5-diphenyltetrazolium bromide (MTT) reduction test, as previously described [36].

For biocompatibility testing, titanium plates of 10 mm × 10 mm × 3 mm, corresponding to one-tenth of the well surface area, were prepared. Uncoated titanium plates (control) or plates covered with HA (HA1, HA2, or HA3) were used. The control for titanium-bound HA was HA powder (HA0), corresponding to the amount of HA on the titanium plate. The absorbance was measured spectrophotometrically using a Multiskan EX plate reader (Thermo Scientific, Waltham, MA, USA) at 570 nm. MTT reduction relative to untreated cells (%) = (absorbance of treated cells/absorbance of untreated cells × 100%) × 100%.

#### 2.2.1. Monocyte Activation Assay

THP1-Blue™ cells (Invitrogen, San Diego, CA, USA), derived from the human THP-1 monocyte cell line, were used to assess whether the HA-coated titanium plates could stimulate monocytes through induction of nuclear factor kappa B (NF-κB). THP1-Blue™ cells were derived from the human THP-1 monocyte cell line by stable integration of an NF-κB-inducible embryonic alkaline phosphatase (SEAP) reporter construct. Activation of NF-κB resulted in the secretion of SEAP, which could be detected spectrophotometrically using Quanti-Blue reagent (Invitrogen, San Diego, CA, USA).

THP1-Blue™ cells were cultured at 37 °C in a 5% $CO_2$ in RPMI-1640 medium supplemented with 10% FBS, 25 mM 4-(2-hydroxyethyl)-1-piperazine-ethanesulfonic acid (HEPES), penicillin/streptomycin (100 U/mL), and 2 mM glutamine (all from Biowest, Nuaillé, France), as well as blastidin (10 µg/mL) (Invitrogen, San Diego, CA, USA), as previously described [37].

The cells were placed in 6-well tissue culture plates ($5 \times 10^5$ cells/mL) and incubated for 24 h under the conditions noted above, in the presence of bare titanium plates or plates covered with HA (HA1, HA2, HA3) or in a milieu of HA powder (HA0). Untreated cells in culture medium alone served as a negative control, whereas cells treated with Escherichia coli lipopolysaccharide (LPS) (1 µg/mL) (Sigma-Aldrich, St. Louis, MO, USA) were taken as a positive control. At the assay end point, 20 µL of each cell culture supernatant was added to 180 µL of chromogen substrate solution (Quanti-Blue reagent, Invitrogen, San Diego, CA, USA) and the SEAP activity as a marker of cell activation was assessed after 4 h. After incubation for 4 h, the absorbance at 650 nm was measured by means of a Multiskan EX plate reader (Thermo Scientific, Waltham, MA, USA).

#### 2.2.2. Bacterial Growth on Hydroxyapatite and Titanium Surface

Bacterial strain *Staphylococcus aureus* 65389 (ATCC, Rockville, MD, USA) was used for the study. Bacteria were taken from a stock solution in glycerin frozen at −80 °C and plated on LB agar (A&A Biotechnology, Gdańsk, Poland). The bacteria were incubated for 18 h at 37 °C. The grown bacterial colonies were then passaged three times under standard conditions to stabilize the strain. A single typical bacterial colony from the third passage was transferred to liquid Luria–Bertani (LB) medium and incubated at 37 °C for 8 h. The tube containing the bacteria was centrifuged (3 min, 5000× *g*). The bacterial sediment was rinsed with sterile physiological saline and the bacteria were centrifuged once more. Thereafter, the supernatant was removed and the optical density of the bacterial suspension was determined using sterile saline on 1 MacFarland scale.

The test materials (bare titanium substrate and HA-coated titanium substrates) were sterilized by autoclaving under standard conditions and drying at 100 °C. Single pieces

(10 mm × 10 mm × 3 mm) of the tested materials (uncoated, sandblasted grade 2 titanium or HA-coated titanium bars) were transferred to a small Petri dish (30 mm in diameter), with the samples coated with HA at the top. LB medium was poured into the Petri dish so that it covered the entire surface of the sample. The medium was then inoculated with the prepared bacterial inoculum and the culture was incubated for 18 h at 37 °C. The test material was rinsed with sterile physiological saline and placed in a sterile Petri dish at 4 °C.

#### 2.2.3. Determination of the Amount of Bacteria Adhered to the Surface of Hydroxyapatite

The Modified Vortex Method was used to determine the amount of bacteria attached to the hydroxyapatite and titanium surface. Briefly, the specimens preincubated with bacteria were intensely rinsed with sterile physiological saline to remove non-adhering bacteria. The samples were then placed in test tube with sterile physiological saline and vortexed vigorously to remove adherent bacteria from the surface. Then, serial dilutions were made to determine the number of colony-forming units (CFU) in 1 mL of bacterial suspension. For this purpose, 100 µL of the diluted bacterial suspension was inoculated on the solid medium and the bacterial colonies grown after incubation at 37 °C for 24 h were counted.

### *2.3. Statistical Analysis*

Differences between the two groups were assessed by the nonparametric Mann–Whitney U test with significance, $p < 0.05$.

## 3. Results and Discussion

Both the HA powder and the deposited coatings morphology were examined by scanning electron microscopy. As shown in Figure 2a, the powder's grains generally had a smooth surface and a spherical shape, which facilitated their transport in the plasma-spraying process. As it turns out, they had a nanostructural nature, being composed of smaller nanograins of a size <100 nm (Figure 2b). A similar structure can be obtained by synthesizing HA using the sol–gel method [35]. Moreover, the high porosity of the grains was also visible on the metallographic specimens of the HA powder grains (Figure 2c). Analysis of the particle size distribution of the HA powder confirmed the significant grain size variation shown in Figure 2a, and the powder parameters were d10 = 3.80 µm, d50 = 69.82 µm, and d90 = 146.30 µm.

XRD analysis confirmed the presence of only hydroxyapatite in the powder. No other forms of calcium phosphate were observed (Figure 3).

Cross-sections of coatings HA1, HA2, and HA3 are shown in Figure 4a–i, respectively, which clearly reveal their lamellar structures. The highly deformed lamellas were characterized by significant internal porosity, which stemmed from the porosity of the HA powder grains. It also resulted, in part, from the significant differentiation of the remelting of HA powder grains depending on their size and position in the plasma stream. In Figure 4d,e cracks were visible between the lamellas, which may have arisen from reduced coating cohesion as a result of the shortest spray distance.

Figure 5 shows the surface structures of the sprayed HA coatings, which are particularly important in the context of biological interactions. Depending on the grain size and its place in the plasma stream, its nanostructure may be preserved and become an element of the created HA coating.

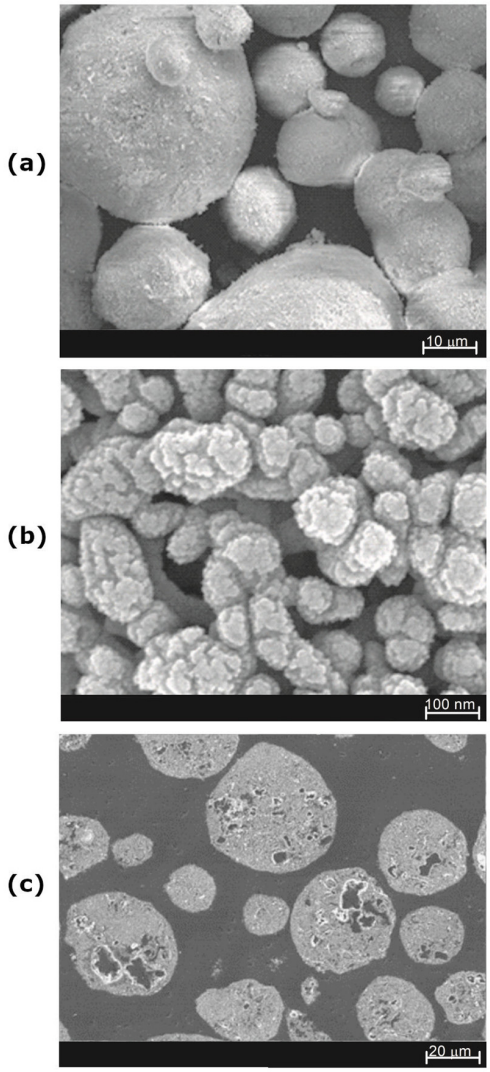


**Figure 2.** Hydroxyapatite (HA) powder grain morphology, (**a**) powder grain surface morphology, (**b**) powder grains cross-section, (**c**) obtained using JEOL JSM-7100 scanning electron microscope (Tokyo, Japan); (**a**) ×500, (**b**) ×10,000, (**c**) ×1000 magnification.

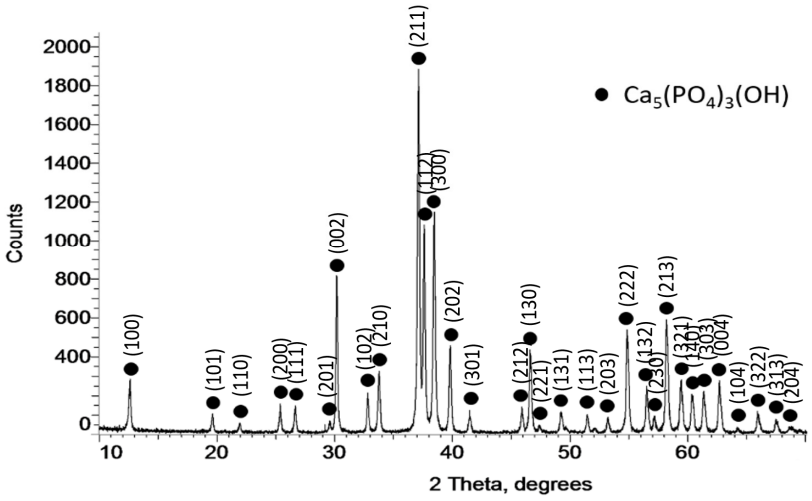


**Figure 3.** X-ray diffraction pattern of hydroxyapatite (HA) powder.

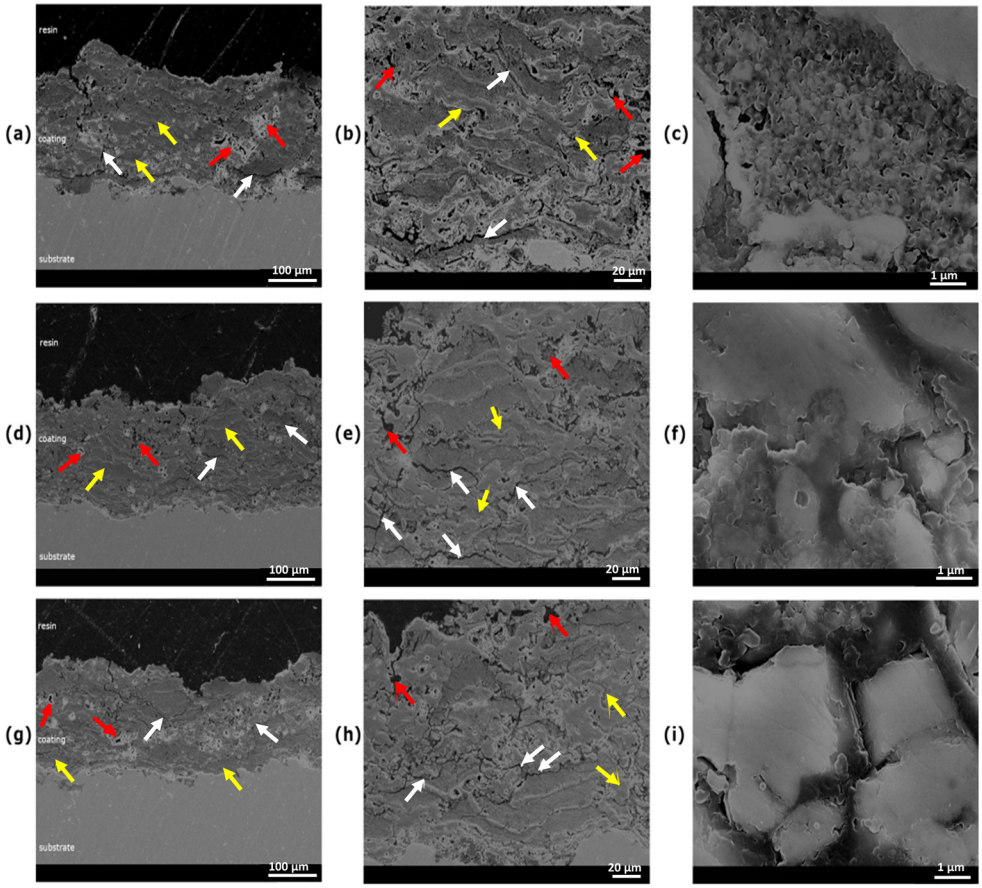


**Figure 4.** Microstructures of hydroxyapatite (HA) coatings ta low and high magnification; (**a**–**c**) HA1, (**d**–**f**) HA2, (**g**–**i**) HA3. Arrows: white–cracks, yellow–deformed lamella, red–pores.

For the HA1 sample, partially preserved nanostructures of powder incorporated into a coating surface are clearly visible, as shown in Figure 5a. On the other hand, the temperature transformed (remelting) HA grains were also visible. However, the remelting process seems to be partial; HA forms characteristic polyhedra. In the HA2 sample, a fully remelted HA grain adjacent to nanostructured elements of the coating was observed, as shown in Figure 4b. Nevertheless, the original, unmelted nano-grains are still visible. The phase of full HA grain remelting is clearly visible in Figure 4c, which reveals a gradual loss of the nanostructure of the HA powder. A similar effect was reported by Shamray et al., but the small amount of grain structure retained differed due to the different type of powder used [30]. No spherical particles were seen. Gkomoza et al. reported similar structures achieved by plasma spraying of the same HA powder (XPT-D-703), but with a higher degree of melting [38]. Primary grain nanostructures were seen to be partially melted.

Based on analysis of the surface morphology, it can be assumed that the abovementioned surface elements were also integral components of HA coatings. The uneven melting of HA powder grains led to changes in phase composition. As shown in Figure 6, in the sprayed HA coatings, a new $Ca_4O(PO_4)_2$ phase appeared, giving rise to small XRD peaks. The obtained results are, therefore, generally consistent with the results obtained in the papers [30,34].

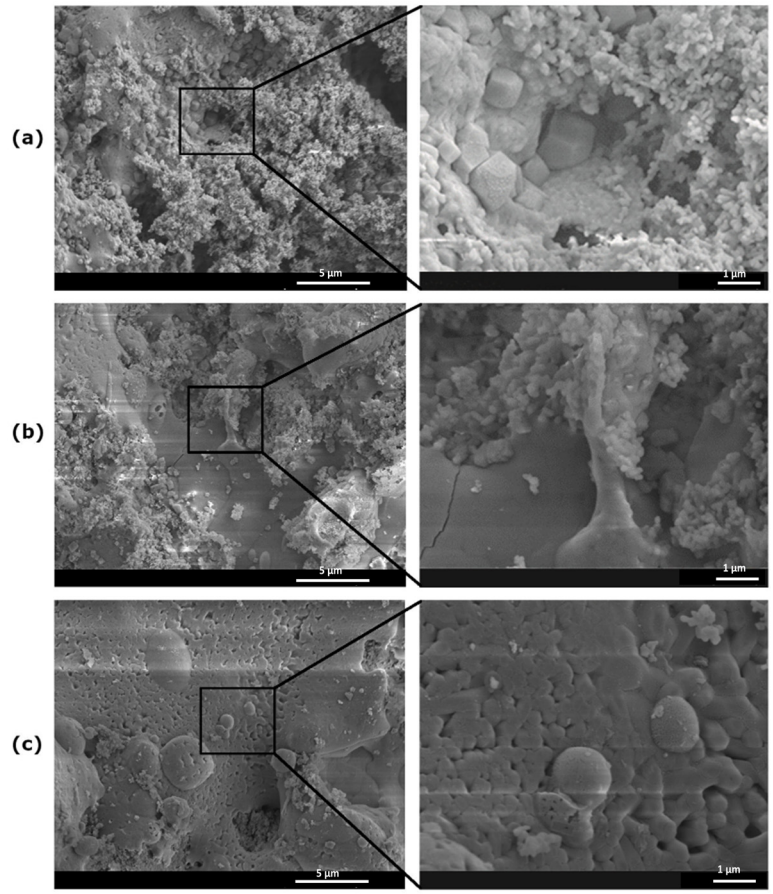


**Figure 5.** Morphologies of the surfaces of HA coatings at low and high magnification; (**a**) HA1, (**b**) HA2, (**c**) HA3.

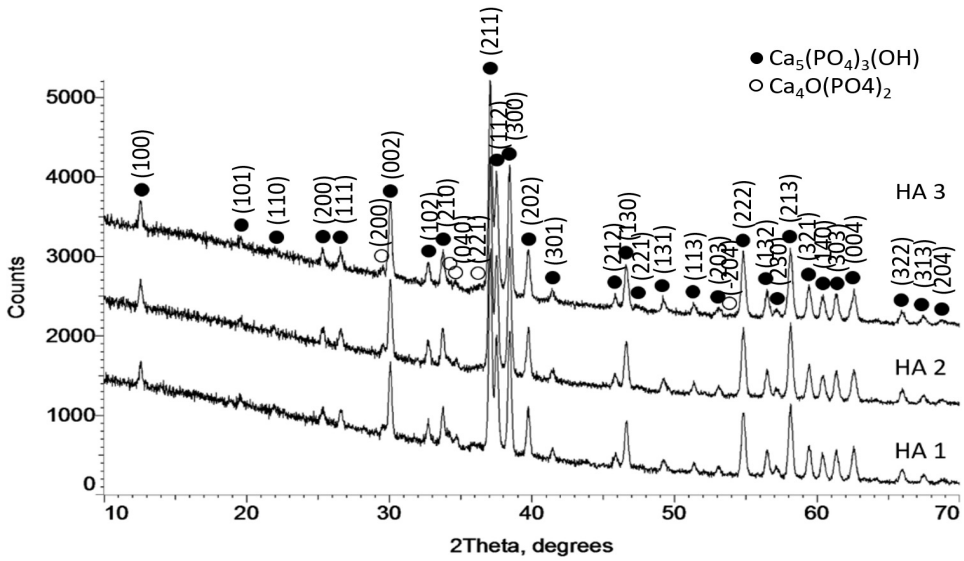


**Figure 6.** XRD patterns of hydroxyapatite (HA) coatings (HA1, HA2, and HA3).

The surface geometry parameters of the plasma-sprayed HA coatings are presented in Table 2, and an exemplary surface geometry of the HA coatings is shown in Figure 7. The results cover an area 1.5 mm × 1.5 mm. Plasma-sprayed HA coatings have a geometry typical of thermally sprayed coatings, which is a consequence of the deformation of the applied powder when it hits the Ti alloys substrate. The largest arithmetic mean defor-

mation of the surface (Sa) was characteristic for HA2 sample (23.2 µm), which proved its greatest expansion. The lower value of this parameter in the case of the HA1 coating could be explained by the shorter spray distance, which resulted in a higher temperature of the sprayed substrate and a greater degree of deformation of the powder grains that hit it. In the case of the HA3 coating sprayed from a distance of 140 mm, the 20% lower value of this parameter was a result of the much longer residence time of the HA powder grains in the plasma stream, which resulted in their greater melting and deformation. The highest value of the Sa, Sq, Sp and Sz parameters in the case of the HA2 were the result of a lower melting of the powder grains (Table 2).

**Table 2.** Surface geometry parameters of hydroxyapatite (HA) coatings (ISO 25178).

| Parameter | Sa µm | Sq µm | Ssk | Sku | Sp µm | Sv µm | Sz µm |
|---|---|---|---|---|---|---|---|
| HA1 | 18.874 ± 1.617 | 23.700 ± 1.858 | 0.319 ± 0.002 | 2.984 ± 0.154 | 89.162 ± 0.426 | 71.030 ± 2.547 | 160.192 ± 3.164 |
| HA2 | 22.486 ± 1.390 | 28.399 ± 1.550 | 0.260 ± 0.175 | 3.042 ± 0.188 | 94.733 ± 6.900 | 96.333 ± 7.153 | 191.067 ± 12.356 |
| HA3 | 18.685 ± 1.615 | 23.657 ± 1.853 | 0.353 ± 0.271 | 3.231 ± 0.458 | 95.604 ± 17.863 | 68.983 ± 1.940 | 164.254 ± 17.811 |

Sa-Arithmetical mean height, Sq-Root mean square height, Ssk-Skewness, Sku-Kurtosis, Sp-Maximum peak height, Sv-Maximum pit height, Sz-Maximum height.

Flatness of the surface, or kurtosis (Sku), increased with increasing spraying distance and degree of powder remelting. It can result in thermal effects on the substrate. Highest (Sp) points increased with spraying distance, but the shallowest (Sv) point value was clearly greater for the HA2 sample. Sz parameters were calculated from the absolute highest and lowest points.

### *3.1. Cell Viability in the Milieu of Tested Biocomposites*

The influence of titanium biocomposites coated with HA (HA1, HA2, HA3) or HA alone (HA0), as well as a bare titanium probe, on the viability of the reference L929 mouse fibroblasts and human Hs68 fibroblasts was assessed by MTT reduction assay, based on the measurement of mitochondrial dehydrogenase activity in the presence or absence of the tested substances. In this assay, the biochemical activity of mitochondrial enzymes was positively correlated with cell viability. The viability of L929 and Hs68 cells incubated in the presence of non-modified titanium plates, HA1-, HA2-, and HA3-coated titanium plates, as well as non-bound HA (HA0), was higher than 70%, meeting the biological safety standard (Figure 8a). Specifically, the viabilities of murine fibroblasts exposed to titanium probes covered with HA1, HA2, HA3, and HA0 were 83 ± 3%, 87 ± 5%, 84 ± 13%, and 84 ± 4%, respectively (Figure 8a(i)). The metabolic activities of human fibroblasts co-cultured with HA1-, HA2-, HA3-, or HA0-coated titanium probes were 89 ± 7%, 90 ± 4%, 89 ± 5%, and 89 ± 3%, respectively (Figure 8a(ii)).

### *3.2. Immunocompatibility of Titanium/HA Biocomposites with THP1-Blue™ NF-κB Human Monocytes*

The immunocompatibilities of a titanium probe alone, or such a probe coated with HA (HA1, HA2, HA3), as well as HA alone (HA0), were evaluated by an in vitro assay with THP1-Blue$^{TM}$ monocytes. It was shown that neither HA1, HA2, or HA3 deposited on titanium plates, nor HA alone (HA0), nor the bare titanium probe stimulated human monocytes (Figure 8b). The concentration of SEAP was similar in cell cultures with tested samples vs. control cell cultures without tested biocomponents (0.28 ± 0.02). Cells responded by SEAP production due to NF-κB activation after exposure to lipopolysaccharide *E. coli* (1 µg/mL), which was used as a positive control of monocyte activation (1.82 ± 0.09) (Figure 8b).

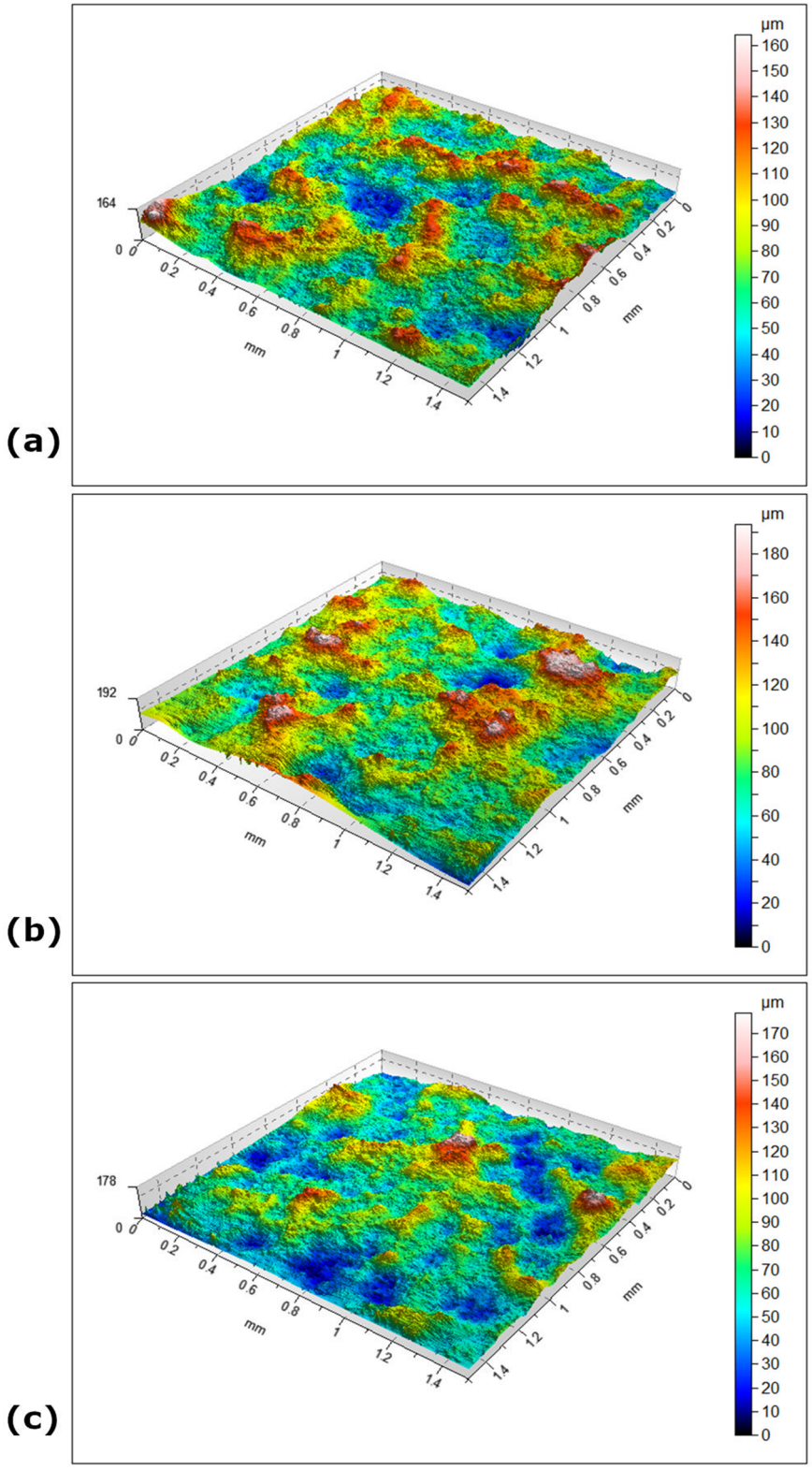


**Figure 7.** Surface geometry of hydroxyapatite coatings (**a**) HA 1, (**b**) HA 2 (**c**) HA 3.

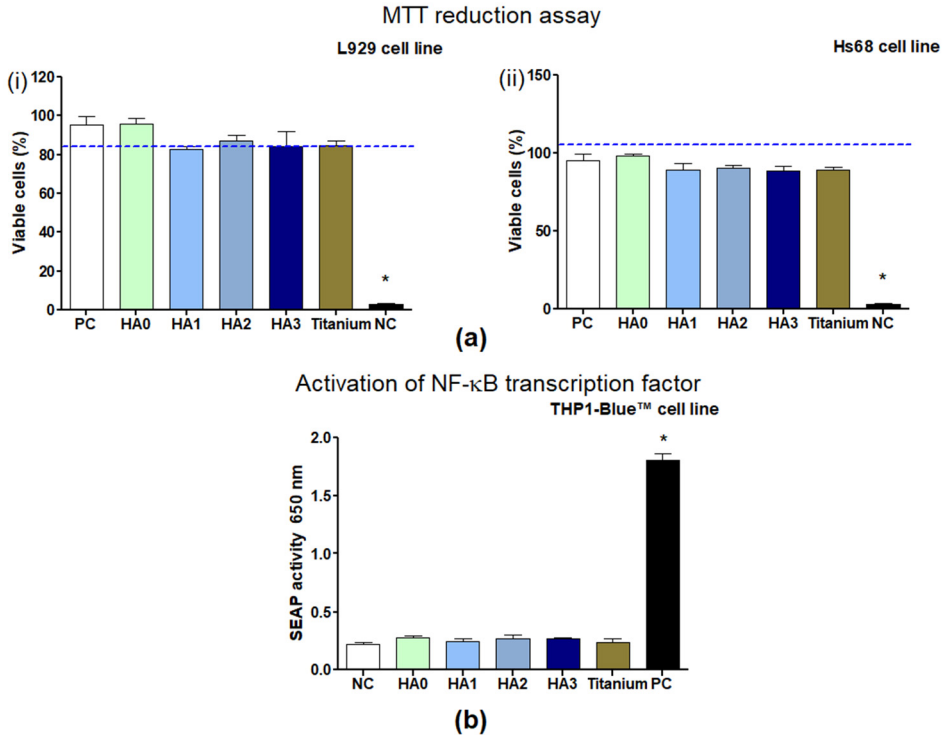


**Figure 8.** Biocompatibility of hydroxyapatite (HA)-coated titanium probes. (**a**) viability of (**i**) murine fibroblasts L929 or (**ii**) human fibroblasts Hs68, incubated for 24 h with bare titanium plates alone, such plates modified with HA (HA1, HA2, HA3), or with HA in solution (HA0), evaluated by 3-(4,5-dimethylthiazol-2-yl)-2,5-diphenyltetrazolium bromide (MTT) reduction assay according to ISO-10993-5:2009. Complete RMPI-1640 medium (cRPMI) was used as a positive control (PC) of cell viability (100% viable cells) and 0.03% $H_2O_2$ as a negative control (NC) of cell viability (100% dead inactive cells). The blue line indicates the minimal percentage of viable cells (70%) required to confirm the biomaterial as non-cytotoxic at the in vitro level C. (**b**) Activation of nuclear factor kappa B (NF-κB) in THP1-Blue™ monocytes incubated for 24 h with bare titanium plates alone, such plates modified with HA (HA1, HA2, HA3), or with HA (powder) in solution (HA0) was determined on the basis of secreted embryonic alkaline phosphatase (SEAP) activation. Cells incubated without composites served as a negative control of the monocyte activation (NC), and monocytes stimulated with lipopolysaccharide (LPS) of *E. coli* served as a positive control (PC). Data are presented as mean ± SD of three separate experiments (six replicates for each experimental variant). Statistical significance: * $p < 0.05$; * untreated cells vs. cells treated with tested biomaterial.

Biocomposites for medical applications destined for implantation or prolonged contact with tissues have had to meet particular in vitro cytocompatibility criteria, even in the early stages of composite optimization (ISO 10993-5:2009). In this study, in addition to standard L929 mouse fibroblasts, which are recommended by ISO standards for biocompatibility assessment of biocomposites, Hs68 human fibroblasts were also examined. The results on the safety of the biomaterials are presented in Figure 8a(i,ii).

The viabilities of target cells exposed to HA powder alone (HA0) or to titanium plates covered with HA (HA1, HA2, HA3) were in line with the ISO criterion of maintaining at least 70% live cells after exposure to the biomaterial for 24 h (ISO 10993-5:2009) (Figure 8a(i,ii)). In the study by Inayat-Hussain et al., the viability of L929 fibroblasts exposed to HA exceeded 75% [39]. Comí et al. also showed a satisfactory absence of cytotoxicity of titanium-HA composite towards Vero or NIH3T3 cells [40].

Monocytes are the most sensitive cells, and upon activation, they rapidly induce a cascade of inflammatory response. Only controlled inflammation leads to revascularization and regeneration of injured tissue. However, strong activation of monocytes by the

components of the biomaterial or contaminants, such as endotoxins, may induce acute inflammation, potentially resulting in pus formation, tissue degradation, and disintegration of cell barriers [41]. THP1-Blue™ cells, like other monocytes, respond to ligands, such as peptides, endotoxins, and glycoconjugates, through toll-like receptors (TLR): TLR-2, TLR-4, TLR-5, TLR-6, and TLR-8. Upon TLR stimulation, NF-κB is activated, and the SEAP enzymatic marker, is subsequently secreted into the cell culture milieu. In this study, bare titanium plates or plates coated with HA did not activate monocytes beyond the negative control value of cells grown in medium alone, which confirmed the immunosafety of the tested biomaterials and the absence of, or very low, endotoxin contamination, which, according to the Food and Drug Agency Guidance as well as the European Medicines Agency, cannot be higher than 0.25 EU in biomaterials in contact with human blood/tissue. Based on our optimization study, the activation of THP1-Blue™ monocytes with 0.25 EU of endotoxin (positive control of monocyte activation) resulted in a significant increase in SEAP production, as shown by an absorbance of 1.8 ± 0.02 at 650 nm. The results on biomaterial safety are presented in Figure 8b

### *3.3. Bacterial Growth on Hydroxyapatite and Titanium SURFACE*

The amounts of washed-out *S. aureus* bacterial cells adsorbed on HA coatings were $1.4 \times 10^6$ and $6 \times 10^4$ for the titanium control. Significant differences between three HA types were shown by the culture method or CFU counting ($p < 0.05$) (Figure 9).

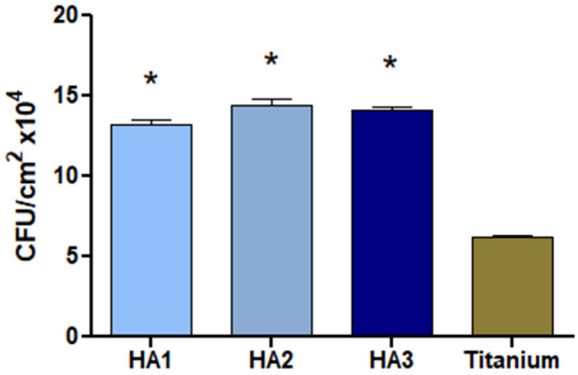


**Figure 9.** Numbers of *S. aureus* cells washed out from HA coatings (HA1, HA2, HA3) and titanium alloy (control). CFU = colony forming unit. Data are presented as mean ± standard deviation (SD) of three separate experiments (six replicates for each experimental variant). Statistical significance: * $p < 0.05$; * HA coatings vs. titanium.

The adhesion of *S. aureus* to the HA surface can be ascribed to the production of adhesins that bind microbial surface components that recognize adhesive matrix molecules (MSCRAMMs) [39]. However, at this stage of our study, it cannot be clearly stated which component of the HA surface plays a similar role as an MSCRAMM. Furthermore, the adhesion of bacteria to HA may depend on non-biological factors. It has been revealed that nanostructured electrophoretic-deposited hydroxyapatite (EPD-HA) is significantly less colonized by *S. aureus* than standard plasma-sprayed hydroxyapatite surfaces, potentially due to the topography of the former. The surfaces coated with EPD-HA are characterized by greater roughness and greater hydrophilicity, and thus, *S. aureus* colonization is more difficult [11]. In the case of the tested HA surfaces, although different conditions of HA spraying on titanium composite resulted in the formation of different nanotopographies of the HA layer, there was no significant difference in the binding of *S. aureus* by the three HA surfaces, as shown by the culture method and CFU counting. Nevertheless, the best results of titanium coating with HA were obtained for a distance of 120 mm, which may be important for the pro-regenerative activity of such biocomposites.

More studies are needed to clarify whether differences in topography of HA layers influence the ability of *S. aureus* bacteria to adhere to an HA surface, and to select the best

method of HA spraying to minimize bacterial adherence, which will increase the safety of HA-coated titanium in regenerative medicine. Further modifications of such biocomposites should also be considered to reduce the binding of bacteria that might otherwise pose a risk of post-operative complications.

There are several limitations in this study that might impact this work. Spraying distance is strongly correlated to other parameters of process. Many factors can influence the final properties of the coating. This not only concerns the process parameters such as the thickness and roughness of the substrate, but the plasma gas composition and gun nozzle surface speed also require further research.

## 4. Conclusions

Plasma-sprayed HA coatings have been deposited by means of an axial injection system at three different distances, which affected the surface geometry, however, it had no effect significant degradation of HA.

A coating sprayed at 120 mm showed the highest values of the surface geometry parameters.

Analysis of the phase composition did not show significant degradation of HA as a result of changing the spray distance; only a few small XRD peaks due to $Ca_4O(PO_4)_2$ appeared.

None of sprayed-HA coating methods affected the biocompatibility of L939 cells and the activation of NF-κB signaling pathway.

The results obtained from the physicochemical and biological characterizations presented in this study suggested that plasma-spraying distance during the HA coating process had a little effect on their biocompatibility. The results obtained for a distance of 120 mm showed a slight increase in the biological properties tested. Because HA constitutes a potentially good, low cost material for joint prostheses, further studies concerning the influence of newly designed HA coatings on bone cell activity, as well as on regeneration properties, are of great importance. However, it appears necessary to first modify such surfaces to improve their antimicrobial properties in order to reduce bacterial infections that may give rise to post-operative complications.

**Author Contributions:** Conceptualization, S.K., W.G., M.C., W.K., Ł.L., W.Ż.; methodology, S.K., W.G., A.G., Ł.L.; validation, S.K., W.G., Ł.L., W.Ż.; formal analysis, W.G.; investigation, S.K., W.G., R.B., A.G., M.C., W.K., Ł.L., W.Ż.; data curation, S.K., W.G., Ł.L.; writing—original draft preparation, S.K., W.G., M.C., W.K., Ł.L., W.Ż.; visualization, S.K., W.G., Ł.L., W.Ż.; supervision; W.Ż.; project administration, W.K., W.Ż.; funding acquisition, W.Ż. All authors have read and agreed to the published version of the manuscript.

**Funding:** Work was partially supported by grant (SUPB.RN. 21.235) from Jan Kochanowski University for WK and project No. 01.1.04.00/1.02.001 SUBB.MCKE.22.004 funded by the Ministry of Education and Science.

**Institutional Review Board Statement:** Not applicable.

**Informed Consent Statement:** Not applicable.

**Data Availability Statement:** The data that support the findings of this study are contained within the article.

**Conflicts of Interest:** The authors declare no conflict of interest.

## References

1. Kaur, M.; Singh, K. Review on titanium and titanium based alloys as biomaterials for orthopaedic applications. *Mater. Sci. Eng. C* **2019**, *102*, 844–862. [CrossRef]
2. Zhang, L.-C.; Chen, L.-Y.; Wang, L. Surface Modification of Titanium and Titanium Alloys: Technologies, Developments, and Future Interests. *Adv. Eng. Mater.* **2019**, *22*, 1901258. [CrossRef]

3. Fukuda, A.; Takemoto, M.; Saito, T.; Fujibayashi, S.; Neo, M.; Yamaguchi, S.; Kizuki, T.; Matsushita, T.; Niinomi, M.; Kokubo, T.; et al. Bone bonding bioactivity of Ti metal and Ti–Zr–Nb–Ta alloys with Ca ions incorporated on their surfaces by simple chemical and heat treatments. *Acta Biomater.* **2010**, *7*, 1379. [CrossRef]
4. Cattini, A.; Łatka, L.; Bellucci, D.; Bolelli, G.; Sola, A.; Lusvarghi, L.; Pawłowski, L.; Cannillo, V. Suspension plasma sprayed bioactive glass coatings: Effects of processing on microstructure, mechanical properties and in-vitro behaviour. *Surf. Coat. Technol.* **2013**, *220*, 52–59. [CrossRef]
5. Liu, X.; Chu, P.K.; Ding, C. Surface modification of titanium, titanium alloys, and related materials for biomedical applications. *Mater. Sci. Eng. R Rep.* **2004**, *47*, 49–121. [CrossRef]
6. Elias, C.N.; Lima, J.H.C.; Valiev, R.; Meyers, M.A. Biomedical Applications of Titanium and its Alloys. *JOM* **2008**, *60*, 46–49. [CrossRef]
7. Nicholson, J.W. Titanium Alloys for Dental Implants: A Review. *Prosthesis* **2020**, *2*, 100–116. [CrossRef]
8. Rack, H.J.; Quazi, J.I. Titanium alloys for biomedical applications. *Mater. Sci. Eng. C* **2006**, *26*, 1269–1277. [CrossRef]
9. Suchanek, K.; Bartkowiak, A.; Gdowik, A.; Perzanowski, M.; Kąc, S.; Szaraniec, B.; Suchanek, M.; Marszałek, M. Crystalline hydroxyapatite coatings synthesized under hydrothermal conditions on modified titanium substrates. *Mater. Sci. Eng. C* **2015**, *51*, 57–63. [CrossRef]
10. Majkowska-Marzec, B.; Rogala-Wielgus, D.; Bartmański, M.; Bartosewicz, B.; Zieliński, A. Comparison of Properties of the Hybrid and Bilayer MWCNTs—Hydroxyapatite Coatings on Ti Alloy. *Coatings* **2019**, *9*, 643. [CrossRef]
11. Montanaro, L.; Arciola, C.R.; Baldassarri, L.; Borsetti, E. Presence and expression of collagen adhesin gene (cna) and slime production in Staphylococcus aureus strains from orthopaedic prosthesis infections. *Biomaterials* **1999**, *20*, 1945–1949. [CrossRef]
12. Mathew, D.; Bhardwaj, G.; Wang, Q.; Sun, L.; Ercan, B.; Geetha, M.; Webster, T.J. Decreased *Staphylococcus aureus* and increased osteoblast density on nanostructured electrophoretic-deposited hydroxyapatite on titanium without the use of pharmaceuticals. *Int. J. Nanomed.* **2014**, *9*, 1775–1781. [CrossRef]
13. Baltatu, M.S.; Vizureanu, P.; Sandu, A.V.; Munteanu, C.; Istrate, B. Microstructural Analysis and Tribological Behavior of Ti-Based Alloys with a Ceramic Layer Using the Thermal Spray Method. *Coatings* **2020**, *10*, 1216. [CrossRef]
14. He, D.; Zhang, X.; Liu, P.; Liu, X.; Chen, X.; Ma, F.; Li, W.; Zhang, K.; Zhou, H. Effect of hydrothermal treatment temperature on the hydroxyapatite coatings deposited by electrochemical method. *Surf. Coat. Technol.* **2020**, *406*, 126656. [CrossRef]
15. Arcos, D.; Vallet-Regí, M. Substituted hydroxyapatite coatings of bone implants. *J. Mater. Chem. B* **2020**, *8*, 1781–1800. [CrossRef]
16. Baltatu, M.S.; Sandu, A.V.; Nabialek, M.; Vizureanu, P.; Ciobanu, G. Biomimetic Deposition of Hydroxyapatite Layer on Titanium Alloys. *Micromachines* **2021**, *12*, 1447. [CrossRef]
17. Awasthi, S.; Pandey, S.K.; Arunan, E.; Srivastava, C. A review on hydroxyapatite coatings for the biomedical applications: Experimental and theoretical perspectives. *J. Mater. Chem. B* **2020**, *9*, 228–249. [CrossRef]
18. Nazirah, R.; Zuhailawati, H.; Hazwani, M.R.S.N.; Abdullah, T.K.; Azzura, I.; Dhindaw, B.K. The Influence of Hydroxyapatite and Alumina Particles on the Mechanical Properties and Corrosion Behavior of Mg-Zn Hybrid Composites for Implants. *Materials* **2021**, *14*, 6246. [CrossRef]
19. Ganvir, A.; Nagar, S.; Markocsan, N.; Balani, K. Deposition of hydroxyapatite coatings by axial plasma spraying: Influence of feedstock characteristics on coating microstructure, phase content and mechanical properties. *J. Eur. Ceram. Soc.* **2021**, *41*, 4637–4649. [CrossRef]
20. Zhou, S.; Bai, Y.; Ma, W.; Chen, W. Suspension Plasma-Sprayed Fluoridated Hydroxyapatite/Calcium Silicate Composite Coatings for Biomedical Applications. *J. Therm. Spray Technol.* **2019**, *28*, 1025–1038. [CrossRef]
21. Yin, X.; Bai, Y.; Zhou, S.; Ma, W.; Bai, X.; Chen, W. Solubility, Mechanical and Biological Properties of Fluoridated Hydroxyapatite/Calcium Silicate Gradient Coatings for Orthopedic and Dental Applications. *J. Therm. Spray Technol.* **2020**, *29*, 471–488. [CrossRef]
22. Gil, J.; Manero, J.M.; Ruperez, E.; Velasco-Ortega, E.; Jiménez-Guerra, A.; Ortiz-García, I.; Monsalve-Guil, L. Mineralization of titanium surfaces: Biomimetic implants. *Materials* **2021**, *14*, 2879. [CrossRef] [PubMed]
23. Ohki, M.; Takahashi, S.; Jinnai, R.; Hoshina, T. Interfacial Strength of Plasma-sprayed Hydroxyapatite Coatings. *J. Therm. Spray Technol.* **2020**, *29*, 1119–1133. [CrossRef]
24. Clavijo-Mejía, G.A.; Hermann-Muloz, J.A.; Rincón-López, J.A.; Ageorges, H.; Muloz-Saldala, J. Bovine-derived hydroxyapatite coatings deposited by high-velocity oxygen-fuel and atmospheric plasma spray processes: A comparative study. *Surf. Coat. Technol.* **2020**, *381*, 125193. [CrossRef]
25. Singh, S.; Pandey, K.K.; Islam, A.; Keshri, A.K. Corrosion behaviour of plasma sprayed graphene nanoplatelets reinforced hydroxyapatite composite coatings in simulated body fluid. *Ceram. Int.* **2020**, *46*, 13539–13548. [CrossRef]
26. Liu, Y.; Lin, G.; Lee, Y.; Huang, T.; Chang, T.; Chen, Y.; Lee, B.; Tung, K. Microstructures and cell reaction of porous hydroxyapatite coatings on titanium discs using a novel vapour-induced pore-forming atmospheric plasma spraying. *Surf. Coat. Technol.* **2020**, *393*, 125837. [CrossRef]
27. Zhang, Z.; Zhao, L.; Ma, Y. Preparing hollow spherical hydroxyapatite powder with a thin shell structure by the plasma process with a heat preservation zone. *Ceram. Int.* **2019**, *45*, 19562–19566. [CrossRef]
28. Shamray, V.F.; Sirotinkin, V.P.; Smirnov, I.V.; Kalita, V.I.; Fedotov, A.; Barinov, S.; Komlev, V. Structure of the hydroxyapatite plasma-sprayed coatings deposited on pre-heated titanium substrates. *Ceram. Int.* **2017**, *43*, 9105–9109. [CrossRef]

29. Li, H.; Ma, Y.; Zhao, Z.; Tian, Y. Fatigue behavior of plasma sprayed structural-grade hydroxyapatite coating under simulated body fluids. *Surf. Coat. Technol.* **2019**, *368*, 110–118. [CrossRef]
30. Liu, X.; He, D.; Zhou, Z.; Wang, G.; Wang, Z.; Guo, X. Effect of post-heat treatment on the microstructure of micro-plasma sprayed hydroxyapatite coatings. *Surf. Coat. Technol.* **2019**, *367*, 225–230. [CrossRef]
31. Gross, K.A.; Berndt, C.C.; Herman, H. Amorphous phase formation in plasma-sprayed hydroxyapatite coatings. *J. Biomed. Mater. Res.* **1998**, *39*, 407–414. [CrossRef]
32. Belka, R.; Kowalski, S.; Żórawski, W. Optical study of plasma sprayed hydroxyapatite coatings deposited at different spray distance. *Proc. SPIE* **2017**, *104454*, 104454R. [CrossRef]
33. Fauchais, P.; Montavon, G.; Lima, R.S.; Marple, B.R. Engineering a new class of thermal spray nano-based microstructures from agglomerated nanostructured particles, suspensions and solutions: An invited review. *J. Phys. D Appl. Phys.* **2011**, *44*, 093001. [CrossRef]
34. Sopyan, I.; Singh, R.; Hamdi, M. Synthesis of nano sized hydroxyapatite powder using sol-gel technique and its conversion to dense and porous bodies. *Indian J. Chem.* **2008**, *47A*, 1626–1631.
35. Unabia, R.B.; Bonebau, S.; Candidato, R.T., Jr.; Jouin, J.; Noguera, O.; Pawłowski, L. Investigation on the structural and microstructural properties of copper-doped hydroxyapatite coatings deposited using solution precursor plasma spraying. *J. Eur. Ceram. Soc.* **2019**, *39*, 4255–4263. [CrossRef]
36. Brzeziński, M.; Kost, B.; Gonciarz, W.; Krupa, A.; Socka, M.; Rogala, M. Nanocarriers based on block copolymers of l-proline and lactide: The effect of core crosslinking versus its pH-sensitivity on their cellular uptake. *Eur. Polym. J.* **2021**, *156*, 110572. [CrossRef]
37. Gonciarz, W.; Matusiak, A.; Rudnicka, K.; Rechciński, T.; Chałubiński, M.; Czkwianianc, E.; Brolnel, M.; Chmiela, M. Autoantibodies to a specific peptide epitope of human Hsp60 (ATVLA) with homology to Helicobacter pylori HspB in H. pylori-infected patients. *APMIS* **2019**, *127*, 139–149. [CrossRef]
38. Gkomoza, P.; Vardavouliasa, M.; Pantelisb, D.I.; Sarafogloub, C. Comparative study of structure and properties of thermal spray coatings using conventional and nanostructured hydroxyapatite powder, for applications in medical implants. *Surf. Coat. Technol.* **2019**, *357*, 748–758. [CrossRef]
39. Inayat-Hussain, S.H.; Rajab, N.F.; Roslie, H.; Hussin, A.A.; Ali, A.M.; Annuar, B.O. Cell death induced by hydroxyapatite on L929 fibroblast cells. *Med. J. Malays.* **2004**, *59*, 176–177.
40. Comín, R.; Cid, M.P.; Grinschpun, L.; Oldani, C.; Salvatierra, N.A. Titanium-hydroxyapatite composites sintered at low temperature for tissue engineering: In vitro cell support and biocompatibility. *J. Appl. Biomater. Funct. Mater.* **2017**, *15*, 176–183. [CrossRef]
41. Mantovani, A.; Biswas, S.K.; Galdiero, M.R.; Sica, A.; Locati, M. Macrophage plasticity and polarization in tissue repair and remodelling. *J. Pathol.* **2013**, *229*, 176–185. [CrossRef] [PubMed]